Analytical and numerical computations of the van der Waals force in complex geometries: Application to the filtration of colloidal particles

Y. Hallez [a,b,*]

[a] Université de Toulouse, INPT, UPS, Laboratoire de Génie Chimique, 118 route de Narbonne, F-31062 Toulouse CEDEX 9, France
[b] CNRS, Laboratoire de Génie Chimique, F-31030 Toulouse, France

HIGHLIGHTS

- An exact solution for the sphere/wedge vdW interaction energy is derived.
- The validity of both simple and new models for sphere/pore interactions is assessed.
- A new numerical tool to compute the van der Waals colloidal interactions is presented.
- An adaptive mesh refinement strategy is used to discretize the solids.

GRAPHICAL ABSTRACT

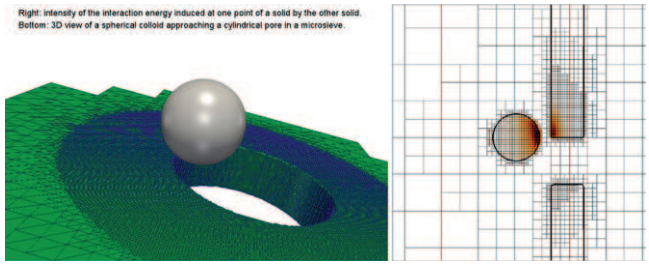

ABSTRACT

Particle capture during the filtration of colloidal dispersions depends on a complex balance between repulsive forces, such as hydrodynamic or electrostatic effects, and attractive forces, amongst them the van der Waals interaction forces. Satisfactory expressions for the latter are thus required in complex geometries. Exact expressions for the geometrical factor involved in the van der Waals interaction energy based on Hamaker's additivity hypothesis are derived for a sphere in interaction with a square wedge, a semi-infinite or finite slit, a semi-infinite slab, a 2D pillar, a rectangular rod, a corner and a rectangular channel. A numerical tool based on an adaptive mesh refinement strategy is presented and used to validate the analytical results. The analytical result for a sphere/wedge system is used to assess the domain of applicability of the sphere/plane model in the vicinity of the edge. The interaction between a sphere and a cylindrical pore in a plate of finite thickness is then simulated and the range of validity of the sphere/wedge system as a model of the sphere/pore system is deduced from the numerical results.

Keywords:
Van der Waals
Analytical
DLVO
Filtration
Colloid
Sphere
Pore
Numerical
Computation
Adaptive mesh

1. Introduction

The evaluation of the van der Waals force or interaction energy between two or more solids is of crucial importance in many academic and industrial problems. Some examples are the (de)stabilization of colloidal suspensions in which an equilibrium between the repulsive electrostatic forces and attractive van der Waals interactions is involved (e.g. [1]), the drying of colloidal films to produce surface coatings, the prediction of protein interactions [2] or the filtration of sub-micronic particles in water treatment [3,4].

In the latter problem, particle capture is the result of a complex interplay between hydrodynamic, electrostatic and van der Waals forces. Let us suppose colloids are not too small and the influence of

* Tel: +33 5 61 55 60 64; fax: +33 5 61 55 61 39.
E-mail address: hallez@chimie.ups-tlse.fr

http://dx.doi.org/10.1016/j.colsurfa.2012.07.033

Brownian motion is moderate. Most of the time electrostatic interactions are repulsive and the Stokes flow transporting a colloid cannot bring it into contact with a wall in a finite time because of repulsive lubrication forces. In short, an external body force is necessary to bring the surfaces into contact. It may be positive or negative buoyancy but its effect is low compared to other forces for sub-micronic objects, or it may be a centrifugal force. Often these two effects are negligible if not absent and the attractive force is mainly due to van der Waals interactions between the colloids and the surface. Hence the particle retention problem is a balance between the attractive van der Waals interactions and all the other repulsive forces. The solution of such a problem is thus dramatically dependent in the quality of the evaluation of van der Waals interactions.

If exact theoretical solutions for these interactions are available for simplified geometries (e.g. [5]), problems depending on the complex shapes of the solids are not tractable analytically. It is necessary either to resort to numerical computations or to do an additivity hypothesis and model the solids as simple spheres, infinite rods, slabs... Concerning the former solution, frequently encountered methods for numerically computing accurate values of the van der Waals interaction energy are direct molecular simulations including N-body interactions, explicit computation of the mean electromagnetic (EM) stress tensor [6], and many other methods discussed in Ref. [7]. These methods provide accurate results, taking into account retardation and non-additive effects, but are however often extremely CPU expensive and/or limited to very simple geometries and/or unable to deal with large solids. The additivity approach, used in the ubiquitous DLVO theory [8,9], has the advantage of rapidly providing a simple result that may be integrated as an elementary brick in a more complex framework (e.g. [10–12]). It may introduce, however, a significant error on the quantitative evaluation of the interactions for at least two reasons: the additivity hypothesis by itself and the simplified geometries for which analytical expressions are available. The additive approach is not adapted for Debye and Keesom interactions, and it should thus be restricted to cases in which (London) dispersion interactions are dominant. In the framework of dispersion interactions, this approximation may lead to large inaccuracies for metals but is expected to provide good estimates for liquids or molecular solids [13]. Covalent solids like diamond or quartz are considered an intermediate case. Generally, this approach is considered to provide results with an error less than 20% when compared to exact solutions [14]. On the other hand, the inability of the standard DLVO sphere or plane models to reproduce experimental or numerical results for complex solid geometries has been recognized by many authors. For instance the stability of a synthetic titania colloidal suspension could not be predicted without taking into account the surface roughness of the particles [15], the molecular recognition processes (linked to van der Waals forces) strongly depend on protein configurations and relative orientations [2], the deposition of particles on rough or nano-patterned surfaces is greatly affected by the geometric details of the surfaces [16–19].

If the accurate non-additive methods are of great interest for understanding the physics of van der Waals interactions, their use is actually an impracticable path when a number of objects interact within a flowing fluid. Indeed the hydrodynamics in a filtration system (and in most engineering systems) are generally not known analytically due to the complex geometry even for model spherical particles and model membranes designed as arrays of well controlled cylindrical pores. In the best case semi-analytical models of trajectories can be integrated numerically [3] and in the worst situations the full Stokes equations must be solved numerically in the filtration geometry at great computational expense. Therefore in studies involving both hydrodynamic and surface forces as a coupled problem, it is necessary to use simple (and fast) models for van der Waals forces, even if it means sometimes cruder models than we wished. In the context of filtration, either an effective distance of capture [3] or a sphere–plane or plane–plane DLVO approximation [20] is generally invoked. The additivity hypothesis is intrinsic to this approach and it seems we need to live with this uncertainty. Thus amongst the two aforementioned error sources involved in DLVO computations one degree of freedom left to improve the van der Waals interaction energy estimation is to reduce the error introduced by simplifications of the actual geometries of the solids. The most classical closed form solutions of van der Waals interactions were obtained for spheres, cylinders, flat plates, disks, parallel slabs or combinations of these geometries (e.g. [26,14,23,28,29]). Examples of geometries previously treated semi-analytically are are proteins (as a collection of spheres) [2], rough surfaces [16], a sphere in a tube [23], a sphere on a nano-patterned plate [19] among many others.

The aim of the present work is twofold: firstly it is to present briefly in Section 2 a new numerical tool able to compute the van der Waals interaction energy within the additivity hypothesis but for arbitrary complex geometries and without any other approximation. The scope of this article is to present this useful numerical method to the colloid community and to illustrate it by an example. The details of the numerical technique will thus be developed more in depth in a journal specialized in numerical analysis. The second aim of the present work is to assess the range of validity of both well-known and new DLVO approximations adapted the context of colloid filtration by using the numerical code as a validation tool. Hence the interaction energy between a sphere and a slit of finite depth is computed analytically and validated numerically in Section 3. The interaction energy between a sphere and a cylindrical pore is then computed numerically in Section 4 and the validity of the sphere/slit approximation as a model of a the real sphere/pore solution is examined.

2. Numerical method

This section describes the numerical approaches underlying the results presented in the rest of the article and implemented in the WITS code developed at LGC. The van der Waals interaction between two solids is estimated with the use of Hamaker's additivity hypothesis. In this context, the interaction energy is computed as a geometrical integral over the volumes $\mathcal{V}_1$ and $\mathcal{V}_2$ of the two particles:

$$E^* = -\frac{A}{\pi^2}\int_{\mathcal{V}_1}\int_{\mathcal{V}_2} f(r)d\mathcal{V}_2\mathcal{V}_1, \tag{1}$$

where A is an effective Hamaker's constant, $f(r) = 1/r^6 = (x^2+y^2+z^2)^{-3}$ (for non-retarded interactions), $x^2 = (x_2 - x_1)^2$, $y^2 = (y_2 - y_1)^2$ and $z^2 = (z_2 - z_1)^2$, and (x_1, y_1, z_1) and (x_2, y_2, z_2) are two points in volumes $\mathcal{V}_1$ and $\mathcal{V}_2$ respectively. In the present work, it is assumed that the retardation/screening effects of the solvent are taken into account at least in a crude way in the Hamaker constant (as advised in [21,14]) or in the form of $f(r)$ ([22] and references therein) and the focus is put on the evaluation of geometrical effects for the reasons detailed in the introduction. Hence results will be presented in terms of $E = E^*/A$.

The integral in Eq. (1) can be evaluated numerically by standard quadrature methods based on the discretization of the particles in small volumes and summation. The standard second order midpoint approximation is used here. To obtain correct results the volumes of these elements must be small, which leads to a great number of integration elements and a heavy computer memory use. As the integral in Eq. (1) consists in six one dimensional integrals the CPU cost is also very high.

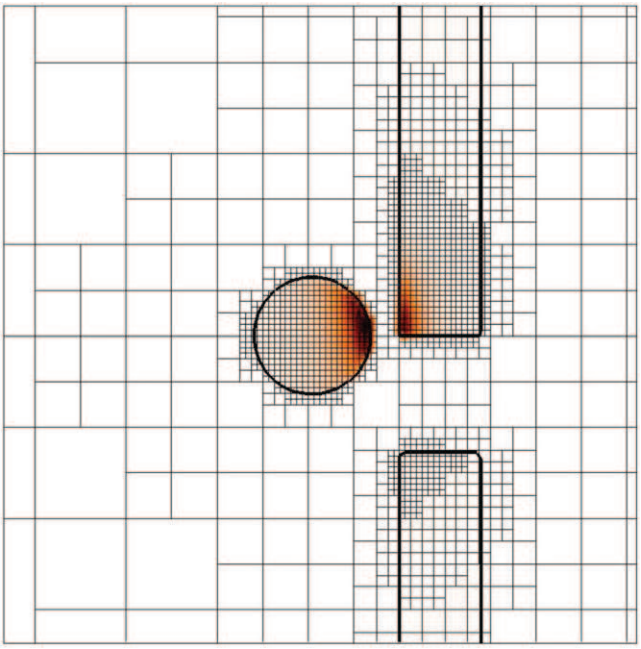

Fig. 1. Octree mesh generated to compute the interaction energy between a sphere and a cylindrical pore. The surfaces of the solids are represented as a thick black line. The colormap represents, at any point of a given solid, the interaction energy between this point and the entire other solid. Darker zones are signs of higher interaction energies. The color scale is skewed to visualize small values.

There are essentially three classical ways to reduce this computational cost, plus a new one described in the next paragraph. When the geometry is relatively simple, it may sometimes be possible to compute analytically part of the integrals involved in Eq. (1), thus reducing the number of integration dimensions (e.g. [23]). In the present work, one of the solids is a sphere and so three integrals have been computed analytically, leaving three other integrals to deal with numerically. A second way to reduce the CPU load is to decrease the number of integration dimensions by converting the integrals on volumes in integrals on surfaces. This is done for example in the Surface Formulation Method [24,25] and in the Surface Element Integration (SEI) method [17,19]. The third way to reduce the CPU cost is to keep the six integrals but split the solids in small elements in an adaptive way, i.e. the smallest elements are located in regions where a high precision is demanded and larger ones are used elsewhere (Fig. 1). It has the advantage of keeping the code able to deal with any geometry, any surface curvature, and without introducing any approximation on the physics.

An additional idea to reduce the computational cost has been developed and implemented in the present code for cases in which the geometry of the solids is so complex that the six integrals have to be computed numerically. It relies on the idea of mapping the volumes of the particles with cubes of different sizes, the cubes being as large as possible far from any interface and smaller and smaller near the interface in order to fit it. This approach requires an analytical form for the interaction energy between two cubes of arbitrary size and position instead of a simple quadrature rule since the elements are not infinitesimal anymore. To our knowledge, this result is not available in the literature. This is why it is derived for the general case of two slabs in Appendix A.

This approach is philosophically close to the SEI method [17,19] which splits the surface of particles in small flat plate elements and then sums the interaction energies for the different plates assuming these energies are closely related to the analytical solution for two parallel semi-infinite solids separated by a gap. Since the present method performs a summation on all the cube couples, it could be termed a "Volume Element Integration" (VEI) method. However, an important distinction is that in the SEI method the flat plate approximation is made for each surface element, which could deteriorate the computation for highly curved surfaces, whereas in the present approach no such approximation is made and any geometry can be handled with an equivalent precision. A method using spheres instead of cubes as mapping elements has also been presented recently (the "Sphere Packing Approach" [27]). Even if it tends to leave holes inside the particle, it may be efficient for some cases, especially for particles with micro-asperities. An hybrid approach using our method in the core of the body and the sphere packing approach near the surface could also be designed easily for an optimal precision/CPU cost ratio in these cases.

A short comment on the adaptive meshing strategy employed here is in order to understand the degree of precision of the numerical computations underlying the results presented in the rest of this article. The mesh, which is based on an "octree" data structure, is refined only in regions of interest and left very coarse elsewhere, so that the computational cost and the memory use are optimized. The quality of the results is then directly linked to the refinement procedure. In the present problem consisting in computing the integral of $1/r^6$, the refinement procedure is the following one:

1. create a uniform coarse mesh of level $n_{\min}$ (usually 4,5 or 6 in the present work) by refining any cell up to this level,
2. compute an estimate of the interaction energy obtained for current mesh level with a prescribed quadrature rule or the VEI,
3. compute the maximum value of $1/r^6$ for all the couples of cells of solid 1 and solid 2,
4. scan all cells i of solid 1 and for each one compute the value of $1/r^6$ with all cells j of solid 2; if $1/r^6 > tol \times \max(1/r^6)$ tag cells i and j for refinement,
5. refine the cells tagged for refinement to reach the next mesh level and go back to point 2.

The only parameter that can be specified by the user is the tolerance *tol*. If it is close to zero, all the cells inside the solids will be refined. No bias will be introduced in the computations but they will be expensive. When *tol* is larger, only cells of solid 1 closer to solid 2 will be refined, and vice versa. Computations will be cheaper since cells outside of the zone of influence of one solid on the other will not be refined. If *tol* is too large, important cells can be left coarse whereas they should have been refined and the results will be poor whatever the final mesh level. A little testing must be done to establish a reliable value of *tol*. In the present work, $tol = 10^{-2}$ permitted to obtain good results for almost all configurations, but not all. Hence $tol = 10^{-3}$ has been set and all the numerical results always converged towards theoretical values, when available, within a few percent. An example of mesh obtained with this value is displayed on Fig. 1, together with a color map representing at any point of a given solid the interaction energy between this point and the entire other solid. It can be checked that this value almost vanishes before the transition to larger cells, which means the results will be obtained with an (high) accuracy linked to the smallest cells size. In practice, the interaction energy was computed for increasing mesh levels automatically and the simulation was stopped when estimations of E for two or three increasing mesh levels differed by less than 1–2%. All the simulations presented in the rest of this article were performed with the three integrals on the sphere volume computed analytically and the adaptive mesh refinement activated for the other solid to spare a maximum of computational time.

3. Interaction between a sphere and a slit of finite depth

3.1. Interaction energy between a sphere and a semi-infinite square wedge

The non-retarded interaction energy between a sphere and a point is

$$E_{s/\text{point}} = -\frac{4}{3}\pi Q_p \beta \frac{a^3}{(d^2-a^2)^3},$$

where Q_p is the number of atom per unit volume, β is the Lifschitz-van der Waals energy constant, a is the sphere radius and d is the distance between the sphere center and the point [23]. The interaction energy between the sphere and the semi-infinite square wedge (a "quarter-space") as depicted on Fig. 2(a) is thus

$$E_{s/w}(a,b,c) = -\frac{4Aa^3}{3\pi}\int_{x=b}^{\infty}\int_{y=c}^{\infty}\int_{z=-\infty}^{\infty}\frac{dxdydz}{(d^2-a^2)^3}, \tag{2}$$

where $d^2 = x^2+y^2+z^2$, $A = \pi^2 Q_p Q_w \beta$ is the effective Hamaker constant and Q_w is the number of atoms per unit volume in the wedge.

The integral in Eq. (2) can be computed analytically. The first integral against z leads to

$$E_{s/w}(a,b,c) = -\frac{Aa^3}{2}\int_{x=b}^{\infty}\int_{y=c}^{\infty}\frac{dxdy}{(x^2+y^2-a^2)^{5/2}}, \tag{3}$$

where x^2+y^2 is the squared distance between the sphere center and a point in the wedge, which is always strictly larger than a^2. The next integration against y gives

$$E_{s/w}(a,b,c) = -\frac{Aa^3}{2}\int_{x=b}^{\infty}\frac{1}{(x^2-a^2)^2}\left[\frac{2}{3}-\frac{c(3(x^2-a^2)+2c^2)}{3(x^2-a^2+c^2)^{3/2}}\right]dx, \tag{4}$$

Note that this expression holds for $|x| \neq a$. The case $x=a$ can be encountered in two very different configurations. In the first one, $c \leq 0$ and $b=a$ (sphere at contact with the wedge "left" plane, see Fig. 2(a)). In this case the interaction energy effectively diverges but this can be solved assuming the contact is never completely achieved. The second configuration is when $c>0$ and $b<a$, i.e. the sphere's foremost point is at least partially on the right side of the wedge's left plane. In this case the points in the wedge corresponding to $x=a$ have nothing special and it can be safely assumed on a physical basis that the integral between b and ∞ can be split in a part between b and a^- and a part between a^+ and ∞, the two parts being finite. The missing part $x=a$ has a zero volume and does not contribute to the integral. Hence we can continue with expression (4). The last integral against x leads to

$$E_{s/w}(a,b\neq\pm a,c) = -\frac{A}{12}\left\{\ln\left[\left(\frac{|c|-a}{|c|+a}\right)^{\text{sign}(c)}\left(\frac{c^2-a^2+|c|\sqrt{b^2+c^2-a^2}+ab}{c^2-a^2+|c|\sqrt{b^2+c^2-a^2}-ab}\right)^{\text{sign}(c)}\left(\frac{|b-a|}{|b+a|}\right)^{1-\text{sign}(c)}\right] - \frac{2abc(b^2+c^2-2a^2)}{\sqrt{b^2+c^2-a^2}(b^2-a^2)(c^2-a^2)}+\frac{2ac}{c^2-a^2}+\frac{2ab}{b^2-a^2}\right\} \tag{5}$$

As expected, this expression cannot be used as is when $b=\pm a$. If $c \leq 0$, the last term in the logarithm makes it diverge, which was expected physically (the sphere touches the leftmost plane of the wedge). If $c>0$, this problematic term vanishes and the second and last terms cancel out exactly, which makes this formula usable in practice. If a human being is able to eliminate the problematic terms analytically, care must be taken when using the formula with a calculator or a computer program. If $b=\pm a$ and $c>0$ it should either be replaced by the corresponding form

$$E_{s/w}(a,b=\pm a,c>0) = -\frac{A}{6}\left\{\ln\left[\frac{c}{c+a}\right]+\frac{ac}{c^2-a^2}\right\} \tag{6}$$

or the value of b should be perturbed slightly to effectively compute $\lim_{b\to a} E_{s/w}(a, b\neq\pm a, c)$ with (5).

Fortunately, formula (5) degenerates to the sphere–plane one for $b\to-\infty$ and $c>a$ or for $c\to-\infty$ and $b>a$. If $c=0$, this expression should be replaced by half the simpler sphere/plane value, which is the exact solution for this symmetric case.

Expression (5) has been validated using the numerical method briefly described in Section 2. A contour map of E obtained with Eq. (5) is drawn on Fig. 3 to get a qualitative idea on its behavior. The interaction energies between a sphere and a square wedge obtained analytically and numerically are reported on Fig. 4 to permit a quantitative comparison. To be perfectly complete some precisions concerning the numerical computations are in order. In all the simulations the sphere radius is $a=0.1$ (this value is completely arbitrary and normalized by the numerical box size). In the sphere/plane simulation the plane is not infinite but is actually a finite slab with a surface area of 1 facing the sphere and a depth of 0.5. It has been checked that larger values of the slab to sphere size ratio did not lead to improvements of the results. The comparison of the analytical results (5) and of the numerical results presented on Fig. 4 is very good. For large negative values of c (sphere in front of a solid wall, see Fig. 2(a)) the sphere/plane model is recovered. For the special case $c=0$ half the sphere/plane value is obtained as expected. Finally for positive values of c (sphere no more in front of a solid plane) the interaction energy is drastically reduced.

Expression (5) for a sphere/wedge interaction can be used to estimate the range of validity of the sphere/plane expression for a particle "far" from the edge of the wedge at $c \ll 0$. A map of the relative error on the interaction energy introduced by the sphere/plane model is represented on Fig. 5. A sphere is drawn as an example of location corresponding to the 10% error. Qualitatively, far from the wedge and close to the wall the sphere/plane model provides very accurate results. For any lateral position c, it is always possible to find a distance to the wall b sufficiently small to make the sphere/plane approximation valid. On the other hand, for positions farther and farther apart from the wall (large b) the sphere/plane approximation is less and less accurate. This is due to the fact that the value of $1/r^6$ between one point of the sphere and the closest point in the wall is not much different from that of the same point in the sphere and the corner of the wall so that the zone of the wall inducing a non-negligible interaction energy is somewhat "truncated" by the pore. This effect can be visualized on Fig. 1. When the sphere is very close to the wall the distance of closest approach is very small and $1/r^6$ decreases sharply so that only a very localized part of the wall contributes to a significant part of the total interaction. Hence the sphere can approach the edge quite closely (small c) without any substantial discrepancy in the sphere/plane model. As a rule of thumb, Fig. 5 shows the sphere/plane approximation to be valid (less than 10% error) for $-c/a>1$ and $b<-0.86c$. For $-c/a \leq 1$ the error grows rapidly with the distance to the wall and the exact solution (5) should be preferred to the sphere/plane approximation.

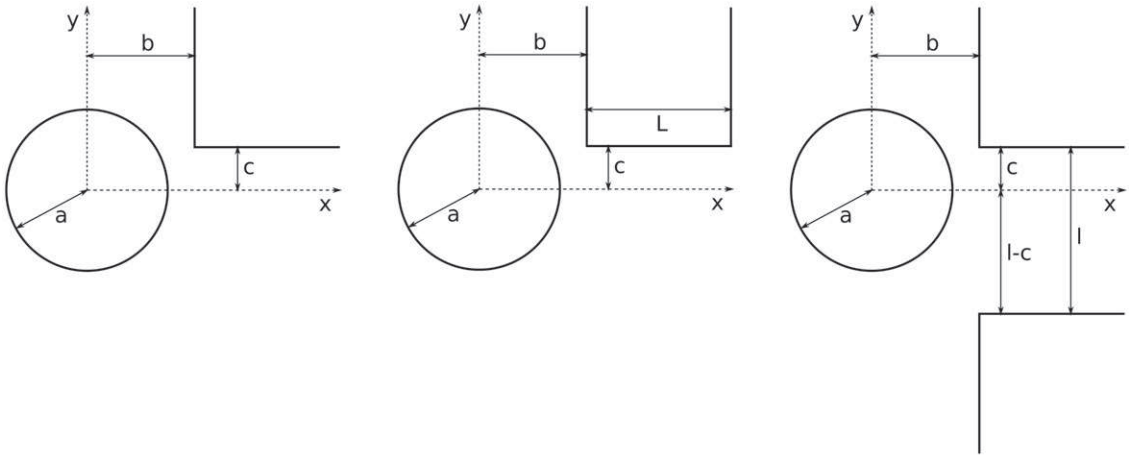

(a) Sphere/square wedge

(b) Sphere/semi-infinite slab

(c) Sphere/infinite slit

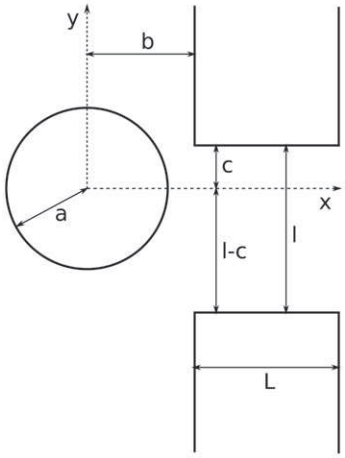

(d) Sphere/finite slit

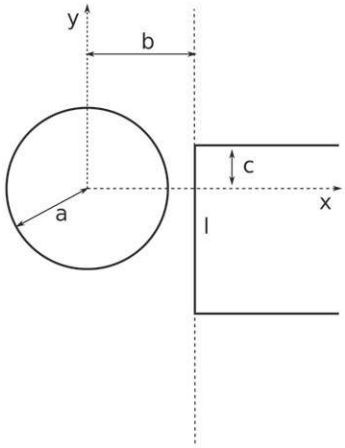

(e) Sphere/2D pillar

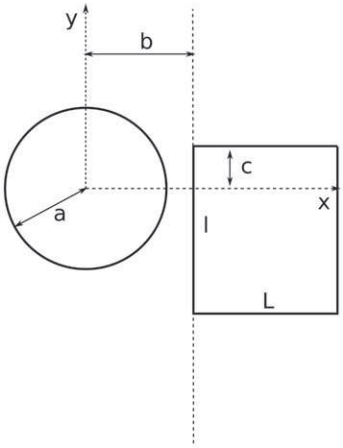

(f) Sphere/infinite rectangular rod

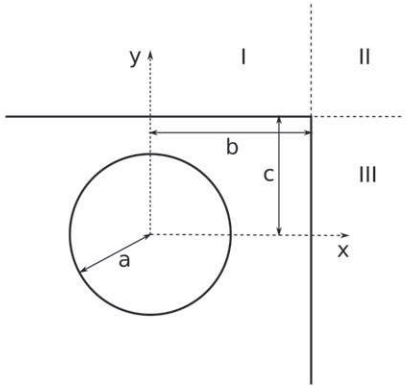

(g) Sphere/square corner

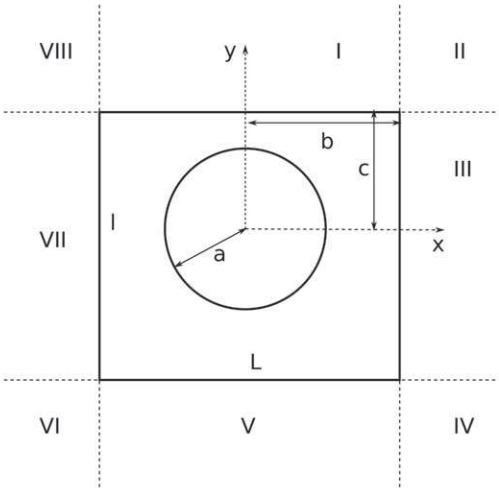

(h) Sphere/rectangular pore

Fig. 2. Schematic view of the sphere/solid problems with the associated geometrical variables.

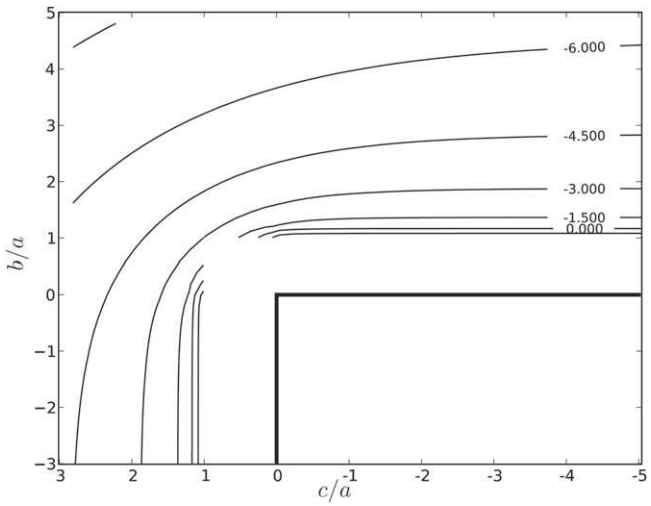

Fig. 3. Contour map of $ln(E)$ obtained with expression (5) for a sphere center placed at coordinates (b, c). The surface of the wedge is drawn as a thick black line. No data was generated for $b \leq a$ and $c \leq a$ for post-processing reasons so the higher level contours are discontinuous near the edge but they are of course continuous in reality.

With the expression of the interaction energy between a sphere and a square wedge known, it is possible to obtain exact relations for several other geometries using the additivity hypothesis. Some of them are listed in the next paragraphs.

3.1.1. Interaction energy between a sphere and a semi-infinite slab

The interaction energy between a sphere and a semi-infinite slab of width L (Fig. 2(b)) is directly related to $E_{s/w}$ as

$$E_{s/i\text{slab}}(a, b, c, L) = E_{s/w}(a, b, c) - E_{s/w}(a, b + L, c) \tag{7}$$

3.1.2. Interaction energy between a sphere and a semi-infinite slit

The interaction energy between a sphere and a semi-infinite slit of width l (Fig. 2(c)) can be expressed by considering the semi-infinite slit as a set of two square wedges:

$$E_{s/i\text{slit}}(a, b, c, l) = E_{s/w}(a, b, c) + E_{s/w}(a, b, l - c) \tag{8}$$

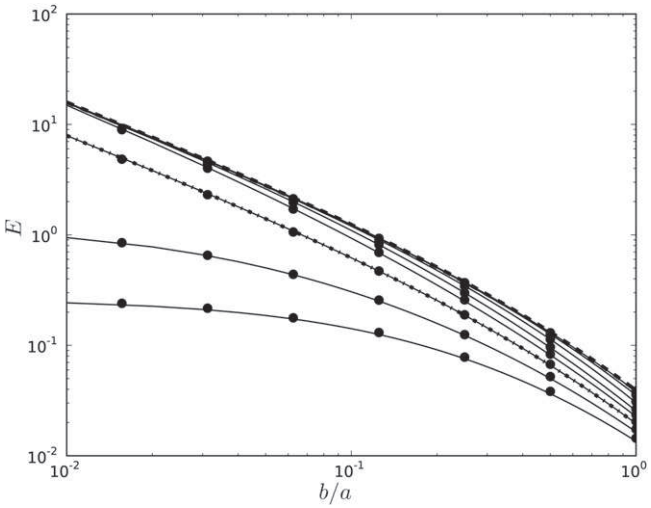

Fig. 4. Interaction energy between a sphere and a square wedge as depicted on Fig. 2(a). Continuous lines: expression (5); dashed line: sphere/plane model; dot-dashed line: half the sphere/plane model; symbols: numerical computations. From top to bottom curve: $c/a = -\infty, -4, -2, -1, -1/2, -1/4, 0, 1/4, 1/2$.

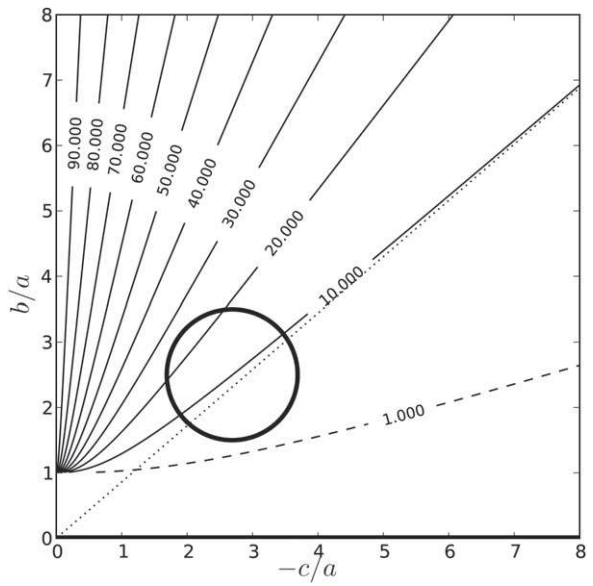

Fig. 5. Contour map of the relative error (%) between the sphere/plane model and the exact expression (5) in the vicinity of the wedge. The plane closest to the sphere is drawn as a black line and extends from $c = 0$ to $-c \to \infty$ (the edge of the wedge is located at (0, 0)). The equation of the dashed line is $b = 0.86(-c)$.

3.1.3. Interaction energy between a sphere and a slit of finite depth

The interaction energy between a sphere and a finite slit of width l and depth L (Fig. 2(d)) can be deduced from the previous result as

$$E_{s/f\text{slit}}(a, b, c, l, L) = E_{s/i\text{slit}}(a, b, c, l) - E_{s/i\text{slit}}(a, b + L, c, l) \tag{9}$$

The validation of Eqs. (8) and (9) against the numerical integration results is presented on Fig. 6. The slit width is $l = 3a$, the distance between the sphere center and the upper plane is $c = 5a/4$ and that between the sphere center and the lower plane is $l - c = 7a/4$. For the finite slit case the depth is $L = a$. The comparison is very good for both geometries. Considering the infinite slit problem (dashed line), the interaction vanishes for large positive b since the sphere is far from the slit entrance. When b is decreased, the magnitude of the interaction energy increases progressively to reach that of a sphere between two planes separated by the slit's width

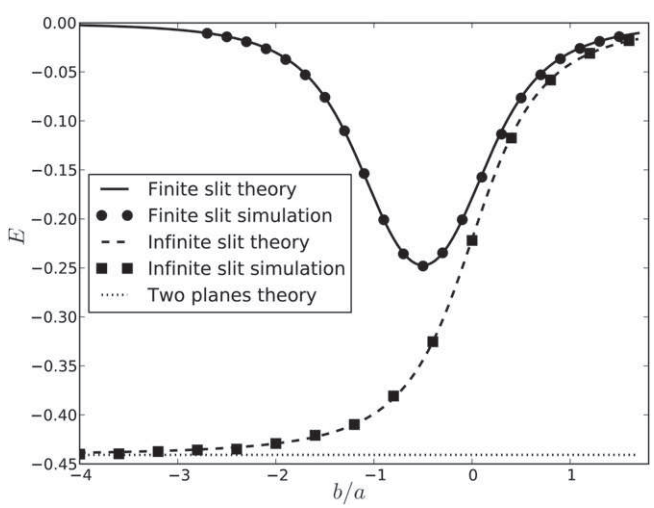

Fig. 6. Interaction energy between a sphere and either an infinite slit (Fig. 2(c)) or a finite slit (Fig. 2(d)). The analytical relation for the infinite (resp. finite) slit is (8) (resp. (9)). The two planes theory (dotted line) is based on the use of the sphere/plane interaction between the sphere and the inner planes of the slit.

(dotted line). This approximation, obviously valid when the sphere is inside the slit and far from its entrance, is seen to provide results within 10% of the exact solution provided the sphere is entirely inside the slit ($b/a < -1$) in the present example. However it should be stressed that this approximation would be satisfactory closer to the slit entrance if the distance between the sphere surface and the slit inner planes were smaller, for the same reasons as those detailed for the sphere/wedge problem. Larger values of $-b$ would be required to achieve the same accuracy for larger l/a ratios, i.e. larger slits compared to the particle size.

The finite slit case shows values similar to those of the semi-infinite slit case when the sphere is before the slit entrance. The interaction energy reaches a maximum at the mid-point between the slit entrance and exit ($b/a = -0.5$). It is theoretically symmetrical against this point but the numerical integration has been performed on both sides to check the variability of the results against the mesh details. The difference between the right and left points is 2–3% at most and often smaller. The maximum value of the interaction energy is only approximately half of that between two planes in the present example due to the finite slit depth. However it should be stressed that this result depends on the particular values of the a/L, a/l and c/l ratios.

3.1.4. Interaction energy for a sphere above a 2D pillar

The interaction energy for a sphere above a 2D pillar of width l (Fig. 2) can be deduced from the previous result and the sphere plane results as

$$E_{s/2D\,\mathrm{pillar}}(a, b, c, l) = E_{s/\mathrm{plane}}(a, b) - E_{s/i\mathrm{slit}}(a, b, c, l) \tag{10}$$

3.1.5. Interaction energy between a sphere and an infinite rectangular rod

The interaction energy between a sphere and an infinite rectangular rod of width L in the x direction and l in the y direction (Fig. 2(f)) can be deduced from the interaction energy for the sphere and a 2D pillar as

$$E_{s/\mathrm{irod}}(a, b, c, l, L) = E_{s/2D\,\mathrm{pillar}}(a, b, c, l) - E_{s/2D\,\mathrm{pillar}}(a, b + L, c, l) \tag{11}$$

3.1.6. Interaction energy between a sphere and a 2D corner

The wall of the surrounding corner can be split in three wedges as depicted on Fig. 2(g). The interaction energy between the sphere and region I is $E_{s/w}(a, c, -b)$, that of region II is $E_{s/w}(a, b, c)$ and that of region III is $E_{s/w}(a, b, -c)$. The total interaction energy is then

$$E_{s/\mathrm{corner}}(a, b, c) = E_{s/w}(a, b, c) + E_{s/w}(a, c, -b) + E_{s/w}(a, b, -c) \tag{12}$$

3.1.7. Interaction energy for a sphere inside an infinite rectangular channel

The rectangular channel (Fig. 2(h)) can be constructed as a superposition of four wedges (regions II, IV, VI and VIII) and four 2D pillars (regions I, III, V, VII). The resulting interaction energy for a channel of width L in the x direction and l in the y direction is:

$$\begin{aligned} E_{s/\mathrm{channel}}(a, b, c, l, L) \;=\; & E_{s/w}(a, b, c) + E_{s/w}(a, b, l - c) + E_{s/w}(a, L - b, c) \\ & + E_{s/w}(a, L - b, l - c) \\ & + E_{s/2D\,\mathrm{pillar}}(a, b, c, l) + E_{s/2D\,\mathrm{pillar}}(a, L - b, c, l) \\ & + E_{s/2D\,\mathrm{pillar}}(a, c, b, L) + E_{s/2D\,\mathrm{pillar}}(a, l - c, b, L) \end{aligned} \tag{13}$$

Relations (12) and (13) are compared to numerical integration results on Fig. 7. In the sphere/corner case the distance between the sphere center and the upper plane is $c/a = 3/2$ and the distance between the sphere center and the right plane b/a is varied. In the sphere/channel case, the channel width is $L = 6a$ in the x direction and its height is $l = 2.75a$ in the y direction. The consistency between

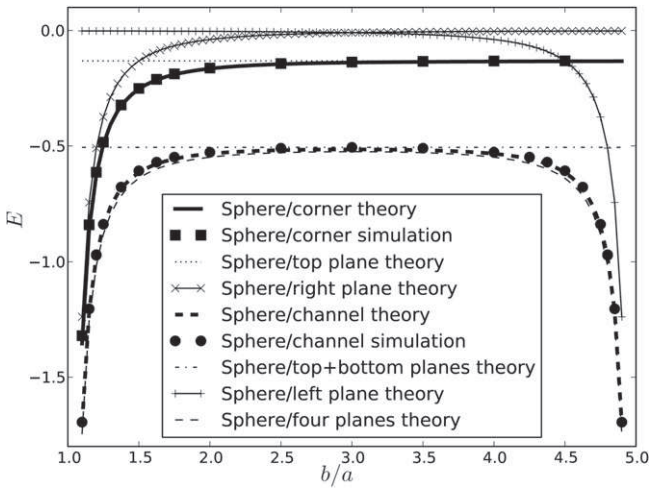

Fig. 7. Interaction energy between a sphere and either a corner (Fig. 2(g)) or a rectangular channel (Fig. 2(h)). The analytical relation for the corner is (12). The analytical solution for a sphere inside a rectangular channel is (13).

the analytical and numerical results is good, which validates Eqs. (12) and (13). Note that Eq. (10) for the interaction between a sphere and a semi-infinite slab is also validated indirectly since it is used in Eq. (13).

Considering the sphere/corner test (thick continuous line on Fig. 7), the solution tends to the sphere/top plane approximation for large values of b/a, i.e. when the sphere is far from the right plane. If the sphere is moved toward the right plane (b/a decreases) the magnitude of the interaction energy increases and reaches that given by the sphere/right plane model for small values of b/a as expected. We may wonder if the sphere/corner interaction could be modeled as the sum of the sphere/upper plane and sphere/right plane interactions. The answer is yes in the present example. It is not plotted on Fig. 7 because the curve would be indistinguishable from the exact sphere/corner solution. The difference can however be seen when zooming in the $1.25 < b/a < 1.75$ zone (not presented here). This difference is due to the fact that with the aforementioned "superposition of planes" model the interaction between the sphere and region II is counted twice. Let us assume a characteristic distance between the sphere and any object is the distance of closest approach between them. The distance of closest approach between the sphere and the upper (resp. right) plane is $c - a$ (resp. $b - a$) and that between the sphere and region II is $\sqrt{b^2 + c^2} - a$. Assume $b = c$ for clarity. The ratio of the distances of closest approach with one plane and the wedge is $r = (b/a - 1)/(\sqrt{2}b/a - 1)$. If the sphere is close to contact with the two planes, $r \to 0$ and the interaction energy is given by the two planes. If the sphere is at a distance large enough such that $b/a \gg 1$, the ratio is $r = 1/\sqrt{2}$, which is finite and close to unity so that the additional wedge contribution included in the sphere/two planes model will not be negligible anymore.

In the sphere/channel test, the solution tends to the sphere/right plane or sphere/left plane model solution when b/a is small (near contact with the right plane) or large (near contact with the left plane), as highlighted on Fig. 7. When the sphere is at mid-distance between the two side planes, the interaction energy is close to that given by the interaction with the upper and lower planes alone. This is due to the large L/l ratio in the present example and is not a general result. A comparison with a sphere/four planes model is provided (thin dashed line). In this model the interaction with the four regions II, IV, VI, VIII (Fig. 2(h)) is counted twice but the approximation is quite good anyway. Once again, it is linked to the geometrical parameters chosen for the present example. This approximation could be less satisfactory for a smaller sphere in the

middle of the channel. In a square channel of width $L = l = Na$, and for a sphere at the center of the channel, the discrepancy between the exact solution and the four planes approximation is 1.5, 10.4, 12.7, 13.1 and 13.1% for $N = 2.1$, 4, 10, 100 and 1000, respectively. Keeping in mind the interaction will be almost totally reduced to zero at a distance of say 10*nm* (at least in water) and that the smallest particles tractable with the present Hamaker approach may have a radius of the order of 1*nm*, the maximum value of $N = L/a$ for a non-negligible interaction will be $O(10)$ at most and the error induced by the four planes approximation will lie within 10% of the "exact" value. Since the additivity hypothesis may induce by itself discrepancies as large as 10–20% with the reality, the four planes approximation can be considered to be an acceptable model for practical use, although one may prefer to use Eq. (13) since it is now available.

4. Interaction between a sphere and a cylindrical pore

The interaction energy between a sphere and a cylindrical pore has been computed by [23] when the sphere is inside the pore. Recently, it has been shown that a single spherical particle approaching a single cylindrical pore was more likely to be captured at two distinct positions [3]. One is slightly away from the pore, above the plate, and the other is right on the pore edge. Both experiments and a trajectory model including hydrodynamics and van der Waals forces (simply as an effective distance of capture) showed these preferential positions of capture but the exact locations were slightly different with the two approaches. The principal motivation of the present work was to obtain a satisfactory expression for the van der Waals interaction between the sphere and the membrane + pore system when the sphere is still outside the pore and very close to its entrance, or even on the edge of the pore where the sphere/plane model is unusable. Moreover, the experiments were conducted using a microsieve as a membrane of 1.4 μm thickness whereas the spheres typically had a radius of 1 μm. The finite depth of the pore thus needs to be taken into account.

Since no analytical solution has been established for a sphere above a plate perforated by a cylindrical hole, the interaction energy has been computed numerically for a plate thickness $L = 1.4a$ and a sphere located right above the pore edge at $c = 0$. For a sufficiently large pore radius ($r_p \gg a$) and a sphere sufficiently close to the pore entrance (small b), the cylindrical pore edge is seen by the sphere as a semi-infinite slab straight edge and relation (7) can be used safely for the sphere/pore interaction. It is however desirable to assess the range of validity of such an approximation in terms of values of r_p/a and b/a.

The sphere/cylindrical pore interaction energy has thus been computed numerically for different pore radii and is compared to the sphere/semi-infinite slab interaction energy (7) on Fig. 8. Simulations have been performed for pore radii r_p ranging from $0.1a$ to $5a$ and for various distances to the plate surface b. One simulation with a semi-infinite slab (circles) has been performed to check the consistency between the numerical results and relation (7). For any pore radius the sphere/plate result is recovered when $b \gg r_p$ (dashed line). Indeed, when the sphere/plate distance is increased the zone of the plate contributing to the total interaction becomes larger and larger compared to the pore size and the existence of the pore can be omitted. This condition is met, of course, for smaller values of the sphere/pore distance when r_p/a is small. Close to contact, if $r_p/a \ll 1$ the interaction energy tend to that of the sphere/plate system but less rapidly than for $b \gg a$. Once again close to contact, if $r_p/a \gtrsim 1$ (the sphere fits exactly inside – or is larger than – the pore) the sphere/semi-infinite slab energy (7) is recovered within 5% and if $r_p/a \gtrsim 2$ it is recovered within 1–2% which is of the order of the precision of the numerical results. Hence the sphere/semi-infinite slab approximation is a very good one for an application to a filtration problem. Indeed, for filtration problems where the pore size is smaller than the particle size, the retention is due to steric effects and the van der Waals force does not play a crucial role. The application of the present work concerns filtration of particles smaller than the pore size, i.e. $r_p/a > 1$ and the discrepancy between the sphere/semi-infinite slab and the actual sphere/pore geometry is always less than 5%, at least for a sphere right above the pore edge ($c = 0$).

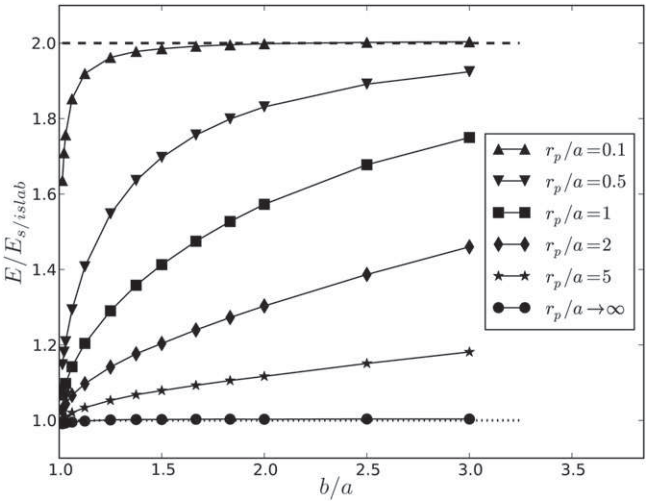

Fig. 8. Interaction energy computed numerically between a sphere and a cylindrical pore in a microsieve of depth $L = 1.4a$ normalized by the interaction energy between a sphere and a semi-infinite slab (Fig. 2(b), Eq. (7)). The different curves correspond to different pore radii r_p. The sphere is located right above the pore edge ($c = 0$). The dashed line is the sphere/plate value ($E_{s/\text{plane}}(a, b) - E_{s/\text{plane}}(a, b + L)$), which is twice the sphere/semi-infinite slab value for $c = 0$.

If the sphere is above the plate ($c < 0$), the radius of curvature of the pore will have even less effect and the approximation is still valid. The sphere/plate approximation may even be used under the conditions detailed in Section 3.1.

When the sphere center lies above the pore orifice ($c > 0$), the influence of the radius of the pore will be more drastic than for the $c = 0$ case presented on Fig. 8. In the microsieve experiments of Lin et al. [3], the most probable position of capture on the pore edge corresponded approximately to a sphere in contact with the pore edge and $b = c$. Numerical computations have been performed with $b = c$ and a distance of closest approach of $a/64$. In this case the discrepancy between the sphere/semi-infinite slab model and the computed "exact" result is 50, 20, 6, and 1% for $r_p/a = 1$, 2, 5, and 10 respectively. Hence in a future experiment it would be desirable to use a pore radius five times as large as the particle radius if the analytical expression is to be used. Note that a numerical computation of the exact interaction energy takes only a few seconds with the code presented in this work so it is always possible to couple it directly to a hydrodynamic trajectory solver for smaller pore sizes.

5. Conclusion

Analytical and numerical evaluations of the van der Waals force between spherical colloidal particles and more or less complex geometries have been proposed. The analytical formulas derived in this article have been validated with the new simulation tool briefly presented in the first section. The range of validity of simple sphere/plane models as approximations of more sophisticated or unknown models for complex geometries involved in colloidal filtration processes has also been assessed by comparison with the simulation results.

The numerical method implemented in the WITS code is based on a classical computation of the six integrals in Eq. (1) for completely arbitrary geometries or on the integration of the three remaining integrals when one of the solids is a sphere and integration on its volume is performed analytically. The originality lies in the use of a so-called octree mesh to discretize the volumes of the solids in an automatic adaptive manner which minimizes the CPU cost without introducing assumptions on the physics. Successive evaluations of the interaction energy for progressively refined meshes enable to monitor the convergence of the numerical integration algorithm and provides an estimate of the numerical error. Simulations were stopped when two successive evaluations differed from less than 1–2%.

An analytical expression for the interaction energy between a sphere and a square wedge has been presented and validated against results obtained numerically. It has been shown that the sphere/plane approximation can be used within a 10% error in the vicinity of the edge of the wedge provided the sphere center is in front of the plane, one radius away from the edge ($c/a < -1$), and provided the distance between the sphere center and the plane respects approximately $b < c$.

Exact expressions for the the interactions between a sphere and a semi-infinite slab, a semi-infinite slit, a finite slit, a 2D pillar, an infinite rectangular rod, a 2D corner and a rectangular channel have been derived from the sphere/plane and sphere/wedge results. They have been validated against results issued from numerical simulations. Combinations of sphere/plane approximations can be used to replace more complex sphere/corner or sphere/channel interactions within 10% error at least in water where the van der Waals forces are rapidly screened.

Since particle capture at the surface of a filtration membrane depends on the van der Waals force between the colloids and the membrane, it would be desirable to know an analytical expression for the interaction energy between a sphere and a cylindrical pore in a plate (when the sphere is outside the pore). Such an expression is however unavailable to our knowledge, hence numerical simulations have been performed to assess the range of validity of the approximation consisting in replacing the cylindrical pore edge by the straight edge of a semi-infinite slab. Close to contact and when the sphere is right above the pore edge, this approximation falls within 10% of the exact result for a pore radius as large as the particle radius and is almost exact for pores radii larger than two particle radii. When the particle is arrested on the pore edge but partially blocking the pore as in Ref. [3], the approximation is valid for pore radii larger that five particle radii.

These results are very encouraging to study the mechanisms of capture of colloidal particles on microsieves. Further experiments will be conducted in collaboration with the fluid dynamicists of IMFT involved in Ref. [3]. The present results will help dimensioning the new experimental setups and, it is believed, enrich the numerical computation of the particles trajectories and positions of capture.

Acknowledgements

I warmly thank Paul Duru, Martine Meireles and Patrice Bacchin for fruitful discussions on this topic. The support of the CALMIP project, which provided access to the "Hyperion" SGI ICE and UV supercomputers, is also greatly acknowledged.

Appendix A. Analytical solution for the non-retarded interaction energy between two slabs located at arbitrary positions

To compute the integral in Eq. (1) with $\mathcal{V}_1$ and $\mathcal{V}_2$ being two slabs of size $a_1 \times b_1 \times c_1$ and $a_2 \times b_2 \times c_2$ respectively, and separated by distances d_x, d_y and d_z in the x, y and z directions respectively (Fig. 9), the method of Ref. [26] is used. Eq. 1 can be specialized in

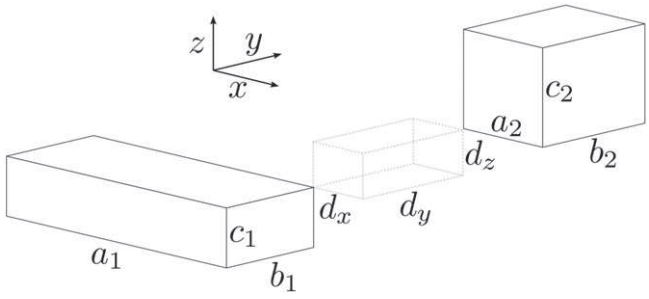

Fig. 9. General configuration of two slabs of size $a_1 \times b_1 \times c_1$ and $a_2 \times b_2 \times c_2$ separated by distances d_x, d_y and d_z in the x, y and z directions respectively.

$$I = -\pi^2 E = \int_0^{a_1} dx_1 \int_{d_x+a_1+a_2-x_1}^{d_x+a_1+a_2-x_1} dx \int_0^{b_1} dy_1 \int_{d_y+b_1+b_2-y_1}^{d_y+b_1+b_2-y_1} dy \int_0^{c_1} dz_1 \int_{d_z+c_1+c_2-z_1}^{d_z+c_1+c_2-z_1} dz\, h(x,y,z), \tag{A.1}$$

where $h(x,y,z) = (x^2+y^2+z^2)^{-3}$.

The second antiderivative of h against z is:

$$h_2(x,y,z) = \frac{3z}{8(x^2+y^2)^{5/2}} \arctan\left[\frac{z}{\sqrt{x^2+y^2}}\right] - \frac{1}{8(x^2+y^2+z^2)(x^2+y^2)} \tag{A.2}$$

This expression is true provided $x^2+y^2 \neq 0$. In the present application there is always at least one space direction, say x, with non-zero integration limits (i.e. slabs are neither in contact nor overlap). Therefore, with this constraint in mind, Eq. (A.2) is always valid. In the integration process, h_2 is evaluated for four values of z before other integrations against y and x are conducted. The second antiderivative of h_2 against y is

$$h_4(x,y,z\neq 0) = -\frac{3y}{16x^3}\operatorname{atan}\left[\frac{y}{x}\right] + \frac{z\left(2y^2+x^2\right)}{8x^4\sqrt{x^2+y^2}} \arctan\left[\frac{z}{\sqrt{x^2+y^2}}\right] + \text{last term with } y,\ z \text{ interchanged} \tag{A.3}$$

or

$$h_4(x,y,z=0) = -\frac{y}{16x^3} \arctan\left[\frac{y}{x}\right] \tag{A.4}$$

Once again, as $x \neq 0$ this expression is always valid. The special case $y = 0$ is now considered (when one face of each slab is in the same plane with normal direction y):

$$h_4(x,y=0,z\neq 0) = \frac{z}{8x^3} \arctan\left[\frac{z}{x}\right] \tag{A.5}$$

or if $y = z = 0$ (when one face of each slab is in the same plane with normal direction y and one face of each slab is in the same plane with normal direction z)

$$h_4(x,y=0,z=0) = 0 \tag{A.6}$$

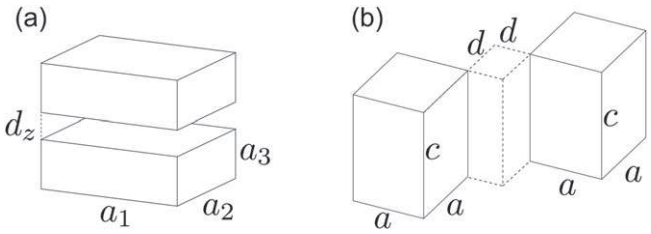

Fig. 10. Geometries treated in Ref. [26]. (a) Two parallel slabs; (b) two slabs with one facing edge.

Table 1
Comparison of the present results with those of [26] for the case of two parallel slabs (Fig. 10(a))

(a, b, c, d_z)	Eq. (21) in [26]	Present (A.1) and (A.7) to (A.10)
(0.5, 0.3, 0.1, 0.2)	$-1.60428336087276 \times 10^{-2}$	$-1.60428336087304 \times 10^{-2}$
(0.1, 0.1, 0.5, 0.3)	$-5.71796733284981 \times 10^{-5}$	$-5.71796733296455 \times 10^{-5}$
(1.0, 2.0, 0.4, 0.1)	-4.15196970900943	-4.15196970900983

Table 2
Comparison of the present results with those of [26] for the case of two skew parallelepipeds with square cross-section (Fig. 10(b))

(a, c, d)	Eq. (25) in [26]	Present (A.1) and (A.7) to (A.10)
(0.1, 0.5, 0.2)	$-3.290827854534256 \times 10^{-4}$	$-3.290827854534263 \times 10^{-4}$
(0.3, 0.1, 0.05)	$-4.144539374852781 \times 10^{-3}$	$-4.144539374851914 \times 10^{-3}$
(1.0, 2.0, 0.1)	-0.133166827308585	-0.133166827308519

The second antiderivative of h_4 against x is

$$h_6(x, y \neq 0, z \neq 0) = \frac{1}{32}\ln\left[\frac{\left(x^2+y^2\right)^3}{x^2\left(x^2+y^2+z^2\right)^2}\right] + \frac{3}{32}\left[\frac{x}{y}-\frac{y}{x}\right]\arctan\left[\frac{y}{x}\right] + \frac{x\left(y^2+z^2\right)^{3/2}}{24y^2z^2}\arctan\left[\frac{x}{\sqrt{y^2+z^2}}\right] + \frac{1}{24}z\left[\frac{1}{x^2}+\frac{1}{y^2}\right]\sqrt{x^2+y^2}\arctan\left[\frac{z}{\sqrt{x^2+y^2}}\right] + \text{last term with } y,\ z \text{ interchanged} \tag{A.7}$$

or

$$h_6(x, y \neq 0, z = 0) = \frac{1}{32}\ln\left[\frac{x^2+y^2}{x^2}\right] + \frac{1}{32}\left[\frac{x}{y}-\frac{y}{x}\right]\arctan\left[\frac{y}{x}\right] \tag{A.8}$$

or

$$h_6(x, y = 0, z \neq 0) = -\frac{1}{16}\ln\left[\frac{x^2+z^2}{x^2}\right] - \frac{1}{16}\left[\frac{x}{z}-\frac{z}{x}\right]\arctan\left[\frac{z}{x}\right] \tag{A.9}$$

or

$$h_6(x, y = 0, z = 0) = x \tag{A.10}$$

The validity of these relations can be checked against the results of Ref. [26] for two parallel slabs (Fig. 10(a)) and two skew parallelepipeds of square cross-section (Fig. 10(b), $a_1 = b_1 = a_2 = b_2 \equiv a$, $c_1 = c_2 \equiv c$, $d_z = -c_1$ and $d_x = d_y \equiv d$). Some results obtained for these two configurations are reported in Tables 1 and 2 respectively. The present results are identical to those of Ref. [26] to machine accuracy.

References

[1] M.-L. Rami, M. Meireles, B. Cabane, C. Guizard, Colloidal stability for concentrated zirconia aqueous suspensions, J. Am. Ceram. Soc. 92 (1) (2009) S50–S56, http://dx.doi.org/10.1111/j.1551-2916.2008.02681.x.

[2] C. Roth, B. Neal, A. Lenhoff, Van der waals interactions involving proteins, Biophys. J. 70 (2) (1996) 977–987, http://www.sciencedirect.com/science/article/pii/S0006349596796418.

[3] J. Lin, D. Bourrier, M. Dilhan, P. Duru, Particle deposition onto a microsieve, Phys. Fluids 21 (7) (2009) 073301, http://dx.doi.org/10.1063/1.3160732, http://link.aip.org/link/?PHF/21/073301/1.

[4] P. Bacchin, A. Marty, P. Duru, M. Meireles, P. Aimar, Colloidal surface interactions and membrane fouling: investigations at pore scale, Adv. Colloid Interface Sci. 164 (1–2, SI) (2011) 2–11, http://dx.doi.org/10.1016/j.cis.2010.10.005.

[5] J. Stenhammar, P. Linse, H. Wennerstrom, G. Karlstrom, An exact calculation of the van der Waals interaction between two spheres of classical dipolar fluid, J. Phys. Chem. B 114 (42) (2010) 13372–13380, http://dx.doi.org/10.1021/jp105754t.

[6] A. Rodriguez, M. Ibanescu, D. Iannuzzi, F. Capasso, J.D. Joannopoulos, S.G. Johnson, Computation and visualization of casimir forces in arbitrary geometries: nonmonotonic lateral-wall forces and the failure of proximity-force approximations, Phys. Rev. Lett. 99 (2007) 080401, http://dx.doi.org/10.1103/PhysRevLett.99.080401, http://link.aps.org/doi/10.1103/PhysRevLett.99.080401.

[7] R.H. French, V.A. Parsegian, R. Podgornik, R.F. Rajter, A. Jagota, J. Luo, D. Asthagiri, M.K. Chaudhury, Y.-m. Chiang, S. Granick, S. Kalinin, M. Kardar, R. Kjellander, D.C. Langreth, J. Lewis, S. Lustig, D. Wesolowski, J.S. Wettlaufer, W.-Y. Ching, M. Finnis, F. Houlihan, O.A. von Lilienfeld, C.J. van Oss, T. Zemb, Long range interactions in nanoscale science, Rev. Mod. Phys. 82 (2010) 1887–1944, http://dx.doi.org/10.1103/RevModPhys.82.1887, http://link.aps.org/doi/10.1103/RevModPhys.82.1887.

[8] L.D. Derjaguin, B.V. Landau, Acta Phys. Chim. U.R.S.S. 14 (1941) 633.

[9] E. Verwey, J. Overbeek, Theory of the Stability of Lyophobic Colloids, Elsevier, Amsterdam, Netherlands, 1948.

[10] M. Fujita, H. Nishikawa, T. Okubo, Y. Yamaguchi, Multiscale simulation of two-dimensional self-organization of nanoparticles in liquid film, Jpn, J. Appl. Phys., Part 1 43 (7A) (2004) 4434–4442, http://dx.doi.org/10.1143/jjap.43.4434.

[11] M. Fujita, Y. Yamaguchi, Multiscale simulation method for self-organization of nanoparticles in dense suspension, J. Comput. Phys. 223 (1) (2007) 108–120, http://dx.doi.org/10.1016/j.jcp.2006.09.001.

[12] B. Schäfer, M. Hecht, J. Harting, H. Nirschl, Agglomeration and filtration of colloidal suspensions with dvlo interactions in simulation and experiment, J. Colloid Interface Sci. 349 (1) (2010) 186–195, http://dx.doi.org/10.1016/j.jcis.2010.05.025, http://www.sciencedirect.com/science/article/pii/S0021979710005527.

[13] H. Wennerstrom, The van der Waals interaction between colloidal particles and its molecular interpretation, Colloids Surf. A 228 (1–3) (2003) 189–195, http://dx.doi.org/10.1016/j.colsurfa.2003.08.006.

[14] J. Israelachvili, Intermolecular and Surface Forces, Academic Press, 1991.

[15] D.R. Snoswell, J. Duan, D. Fornasiero, J. Ralston, Colloid stability of synthetic titania and the influence of surface roughness, J. Colloid Interface Sci. 286 (2) (2005) 526–535, http://dx.doi.org/10.1016/j.jcis.2005.01.056, http://www.sciencedirect.com/science/article/pii/S0021979705000652.

[16] L. Suresh, J.Y. Walz, Effect of surface roughness on the interaction energy between a colloidal sphere and a flat plate, J. Colloid Interface Sci. 183 (1) (1996) 199–213, http://dx.doi.org/10.1006/jcis.1996.0535, http://www.sciencedirect.com/science/article/pii/S0021979796905354.

[17] S. Bhattacharjee, J. Chen, M. Elimelech, DLVO interaction energy between spheroidal particles and a flat surface, Colloids Surf., A 165 (1–3) (2000) 143–156, http://dx.doi.org/10.1016/S0927-7757(99)00448-3.

[18] E. Hoek, G. Agarwal, Extended dlvo interactions between spherical particles and rough surfaces, J. Colloid Interface Sci. 298 (2006) 50–58.

[19] E. Martines, L. Csaderova, H. Morgan, A.S.G. Curtis, M.O. Riehle, DLVO interaction energy between a sphere and a nano-patterned plate, Colloids Surf. A 318 (1–3) (2008) 45–52, http://dx.doi.org/10.1016/j.colsurfa.2007.11.035.

[20] M.-M. Kim, A. Zydney, Effect of electrostatic, hydrodynamic, and brownian forces on particle trajectories and sieving in normal flow filtration, J. Colloid Interface Sci. 269 (2004) 425–431.

[21] W. Russel, D. Saville, W. Schowalter, Colloidal Dispersions, Cambridge University Press, 1989.

[22] A. Anandarajah, J. Chen, Single correction function for computing retarded van der waals attraction, J. Colloid Interface Sci. 176 (2) (1995) 293–300, http://dx.doi.org/10.1006/jcis.1995.9964, http://www.sciencedirect.com/science/article/pii/S002197978579964X.

[23] S. Bhattacharjee, A. Sharma, Lifshitz-van der Waals energy of spherical particles in cylindrical pores, J. Colloid Interface Sci. 171 (2) (1995) 288–296, http://dx.doi.org/10.1006/jcis.1995.1183, http://www.sciencedirect.com/science/article/pii/S0021979785711836.

[24] C. Argento, A. Jagota, W. Carter, Surface formulation for molecular interactions of macroscopic bodies, J. Mech. Phys. Solids 45 (7) (1997) 1161–1183, http://dx.doi.org/10.1016/S0022-5096(96)00121-4, http://www.sciencedirect.com/science/article/pii/S0022509696001214.

[25] P. Yang, X. Qian, A general, accurate procedure for calculating molecular interaction force, J, Colloid Interface Sci. 337 (2) (2009) 594–605, http://dx.doi.org/10.1016/j.jcis.2009.05.055, http://www.sciencedirect.com/science/article/pii/S0021979709006262.

[26] G.D. Rocco, W. Hoover, On the interaction of colloidal particles, Proc. Natl. Acad. Sci. 46 (1960) 1057.
[27] L. Zhang, J. Cecil, D. Vasquez, J. Jones, B. Garner, Modeling of van der Waals forces during the assembly of micro devices, automation science and engineering, in: CASE'06. IEEE International Conference, 2006.
[28] S.W. Montgomery, M.A. Franchek, V.W. Goldschmidt, Analytical dispersion force calculations for nontraditional geometries, J. Colloid Interface Sci. 227 (2000) 567–584.
[29] V.A. Parsegian, Van Der Waals Forces: A Handbook for Biologists, Chemists, Engineers, and Physicists, Cambridge University Press, 2006.